The Astronomical Journal, 167:56 (13pp), 2024 February https://doi.org/10.3847/1538-3881/ad0bfd

The POKEMON Speckle Survey of Nearby M Dwarfs. II. Observations of 1125 Targets

Catherine A. Clark[1,2], Gerard T. van Belle[3], Elliott P. Horch[4], Michael B. Lund[2], David R. Ciardi[2], Kaspar von Braun[3], Jennifer G. Winters[5,6], Mark E. Everett[7], Zachary D. Hartman[8], and Joe Llama[3]
[1] Jet Propulsion Laboratory, California Institute of Technology, Pasadena, CA 91109, USA; catherine.a.clark@jpl.nasa.gov
[2] NASA Exoplanet Science Institute, IPAC, California Institute of Technology, Pasadena, CA 91125, USA
[3] Lowell Observatory, 1400 West Mars Hill Road, Flagstaff, AZ 86001, USA
[4] Southern Connecticut State University, 501 Crescent Street, New Haven, CT 06515, USA
[5] Bridgewater State University, 131 Summer Street, Bridgewater, MA 02324, USA
[6] Center for Astrophysics, Harvard & Smithsonian, 60 Garden Street, Cambridge, MA 02138, USA
[7] NSF's National Optical-Infrared Astronomy Research Laboratory, 950 N. Cherry Avenue, Tucson, AZ 85719, USA
[8] Gemini Observatory/NSF's NOIRLab, 670 A'ohoku Place, Hilo, HI 96720, USA
Received 2023 September 22; revised 2023 November 6; accepted 2023 November 10; published 2024 January 11

Abstract

Stellar multiplicity is correlated with many stellar properties, yet multiplicity measurements have proven difficult for the M dwarfs—the most common type of star in our galaxy—due to their faintness and the fact that a reasonably complete inventory of later M dwarfs did not exist until recently. We have therefore carried out the Pervasive Overview of "Kompanions" of Every M dwarf in Our Neighborhood (POKEMON) survey, which made use of the Differential Speckle Survey Instrument on the 4.3 m Lowell Discovery Telescope, along with the NN-EXPLORE Exoplanet Stellar Speckle Imager on the 3.5 m WIYN telescope. The POKEMON sample is volume limited from M0V through M9V out to 15 pc, with additional brighter targets at larger distances. In total, 1125 targets were observed. New discoveries were presented in the first paper in the series. In this second paper in the series, we present all detected companions, gauge our astrometric and photometric precision, and compare our filtered and filterless speckle observations. We find that the majority (58.9%) of the companions we detect in our speckle images are not resolved in Gaia, demonstrating the need for high-resolution imaging in addition to long-term astrometric monitoring. Additionally, we find that the majority (73.2%) of simulated stellar companions would be detectable by our speckle observations. Specifically within 100 au, we find that 70.3% of simulated companions are recovered. Finally, we discuss future directions of the POKEMON survey.

Unified Astronomy Thesaurus concepts: M dwarf stars (982); Binary stars (154); High angular resolution (2167); Low mass stars (2050); Solar neighborhood (1509)

Supporting material: machine-readable tables

1. Introduction

The smallest, coolest, faintest stars—the M dwarfs—are a microcosm of stellar astrophysics. The M-dwarf spectral class extends from the hydrogen burning limit of 0.08 $M_{\odot}$ (Baraffe & Chabrier 1996) at the bottom of the main sequence to over half the mass of the Sun–nearly a factor of 8. Our low-mass neighbors also span nearly a factor of six in radius and over two orders of magnitude in luminosity (Pecaut & Mamajek 2013). Additionally, the M dwarfs have lifetimes on the order of the age of the Universe (Laughlin et al. 1997), and remain active and rapidly rotating for longer than stars of earlier spectral types (e.g., Popinchalk et al. 2021). Furthermore, the M dwarfs comprise over 70% of stars in our Galaxy (Henry et al. 2006; Winters et al. 2015)and 75% of the stars within 10 pc (Henry et al. 2018), even though not a single one is visible to the naked eye (Shields et al. 2016). The M dwarfs are thus critical to our understanding of stellar astrophysics, and, in particular, the solar neighborhood.

Stars of every spectral type preferentially form in groups (e.g., Lada et al. 1991). The size of these groups ranges from binary-star systems to clusters containing hundreds of thousands of stars. Multiplicity has been found to be correlated with multiple stellar properties; for example, higher-mass stars are more likely to be found in multi-star systems (Mason et al. 2009; Raghavan et al. 2010; Duchêne & Kraus 2013; Winters et al. 2019), and older stars are less likely to be found in multi-star systems (Mason et al. 1998). Binarity can also affect stellar evolution for stars of all masses (e.g., Iben 1991). Understanding the rate and properties of stellar companions is therefore critical to our understanding of the stars themselves, in particular for the M dwarfs due to their high occurrence in our Galaxy.

Understanding stellar multiplicity is also critical to the detection and characterization of exoplanets. Specifically, determining the occurrence rate of planets is highly dependent on an understanding of the multiplicity of the host stars (Dressing & Charbonneau 2015). Known multiplicity is particularly crucial for characterizing exoplanets detected using the transit method. Transit detections from large field-of-view pixel instruments aboard missions such as the Transiting Exoplanet Survey Satellite (Ricker et al. 2015) can lead to erroneous inferences of the planetary properties if unknown secondary companions are contaminating the light curve. Calculations of planet statistics—and thus our understanding of quantities like $\eta_{\oplus}$—therefore hinge critically on the accurate determination of stellar multiplicity (Ciardi et al. 2015).

A number of surveys have been conducted over the past few decades to quantify and understand the rate and properties of the stellar companions that the M dwarfs host (e.g., Henry 1991; Law et al. 2008; Janson et al. 2012; Jódar et al. 2013; Ward-Duong et al. 2015; Winters et al. 2019; Cifuentes 2023). However, many of these studies were limited by the size of their sample, due to the fact that the M dwarfs are quite faint in the optical, and that a reasonably complete inventory of later M dwarfs did not even exist until recently (Kirkpatrick et al. 2014; Luhman & Sheppard 2014; Winters et al. 2021). Additionally, many of these studies were not sensitive to close-in stellar companions due to the resolution limits of the surveys. Close-in companions are known to affect planet formation mechanisms (Haghighipour & Raymond 2007; Jang-Condell 2015; Rafikov & Silsbee 2015a, 2015b), and it has been shown that both solar-type (e.g., Howell et al. 2021) and M-type (Clark et al. 2022a) exoplanet host stars have fewer close-in stellar companions than their non-planet-hosting counterparts. A complete census of M-dwarf companions at all separations is therefore necessary to determine statistics on their properties and occurrence rates. This presents an opportunity to use high-resolution imaging to survey a large number of M dwarfs and their companions at separations down to the diffraction limit.

We have therefore carried out the Pervasive Overview of "Kompanions" of Every M dwarf in Our Neighborhood (POKEMON) speckle survey of nearby M dwarfs. The POKEMON survey is volume limited out to 15 pc from M0V through M9V, with additional brighter targets at larger distances. In total, we have imaged 1125 M dwarfs at diffraction-limited resolution, and we have detected companions to 151 of these targets. The first paper in the series (Clark et al. 2022b) presented the new discoveries, and this second paper in the series presents all detections from the POKEMON survey.

In Section 2, we describe how we defined the POKEMON sample, our observational routine, and our data-reduction process. In Section 3, we present the stellar companions detected throughout the POKEMON survey and examine our astrometric and photometric precision. We also compare our filtered and filterless speckle observations. In Section 4, we evaluate the effect of stellar multiplicity on Gaia astrometry and assess any potentially missed companions. Finally, in Section 5, we summarize our conclusions and detail the future work to be done on the POKEMON survey.

2. Observations

In this section, we describe how we defined the POKEMON sample. We also characterize our observational routine and our data-reduction process.

2.1. Definition of the Sample

The underlying, essential goal of our target-selection process was to provide an as complete as possible sample of M dwarfs out to 15 pc, with special care taken to include the previously overlooked later-type M dwarfs. Assuming a homogeneous distribution of stars in the solar neighborhood, targets from Gaia or other catalogs can be reviewed to investigate whether their number increases linearly with volume or with the cube of distance (d). This is known as a d^3 trend. If a catalog is volume complete, then the d^3 trend should remain constant with increasing volume; when a catalog overlooks faint targets, there are deviations from this trend. An examination of the Catalog of Nearby Stars (or CNS3; Gliese & Jahreiß, 1991) indicated a possible deviation from the targets per unit volume d^3 line at 15 pc, with a definite fall-off trend (i.e., incompleteness) at 25 pc. A number of newer catalogs were therefore cross-referenced to eliminate as much incompleteness as possible. This included nearby neighbor discoveries from RECONS (Henry et al. 2006; Winters et al. 2015) and the Two Micron All Sky Survey (2MASS; Skrutskie et al. 2006). Of particular relevance were the results from the AllWISE Motion Survey as reported by Kirkpatrick et al. (2014) and Luhman & Sheppard (2014), which had found 3525 and 762 high-proper-motion objects, respectively. Using the spectral type–color relationships from Luhman & Sheppard (2014), we identified ∼350 additional potential objects with colors indicating spectral types between M4V and M9V. Additional surveys that were cross-referenced include the Database of Ultracool Parallaxes based on the Hawaii Infrared Parallax Program (Dupuy & Liu 2012), the CARMENES input catalog (Alonso-Floriano et al. 2015), the APOGEE input catalog (Deshpande et al. 2013), and the 2016 release of the Pan-STARRS Parallax and Proper Motion Catalog (Waters et al. 2015), which had the specific focus of identifying nearby low-mass stars (Magnier et al. 2015).

At that time, the speckle cameras available to the POKEMON survey were located at Northern Hemisphere facilities, necessitating a decl. cut of $\delta > -30°$. A cut at $I < 15.5$ was also necessary for most objects due to the faint limit of the instruments. In total, our sample consists of 1125 M dwarfs north of $\delta > -30°$, brighter than $I = 15.5$ mag, and within ∼100 pc (Figure 1). We note that the sample size is updated from the previous paper in the series.

We characterize the 1125 stars in the POKEMON sample in Table 1, where we include the 2MASS ID or name, Gaia Data Release 3 (DR3; Gaia Collaboration et al. 2023) ID, Gaia G magnitude, Gaia G_{RP} magnitude, parallax-derived distance, reference for the distance, Gaia renormalized unit weight error (RUWE) value, and the Gaia ipd_frac_multi_peak (IPDFMP) value. We also note whether the target had companions detected by us.

In Figure 2, we show histograms of the distances and absolute G_{RP} magnitudes for the targets in the POKEMON sample. We use the absolute G_{RP} magnitudes and the mass–magnitude relation from Giovinazzi & Blake (2022) to estimate masses for the POKEMON targets.

Using the apparent G magnitudes from Gaia, the stellar distances, and the reference stellar properties from Pecaut & Mamajek (2013), we estimate spectral types for the POKEMON targets in Table 2. We note that some of the POKEMON targets are estimated to be either K dwarfs or L dwarfs; the fourth paper in the series will provide homogeneous spectral types for all POKEMON targets, allowing for more accurate stellar characterization, and establishing the M-dwarf multiplicity rate by spectral subtype through M9V for the first time.

2.2. Observational Routine

We imaged the 1125 M dwarfs in the POKEMON sample over 50 nights between UT 2017 April 7 and UT 2020 February 10. These observations were mainly carried out using the Differential Speckle Survey Instrument (DSSI; Horch et al. 2009) on the 4.3 m Lowell Discovery Telescope (LDT; Levine et al. 2022) located in Happy Jack, AZ. We also used the NN-EXPLORE Exoplanet Stellar Speckle Imager (NESSI;

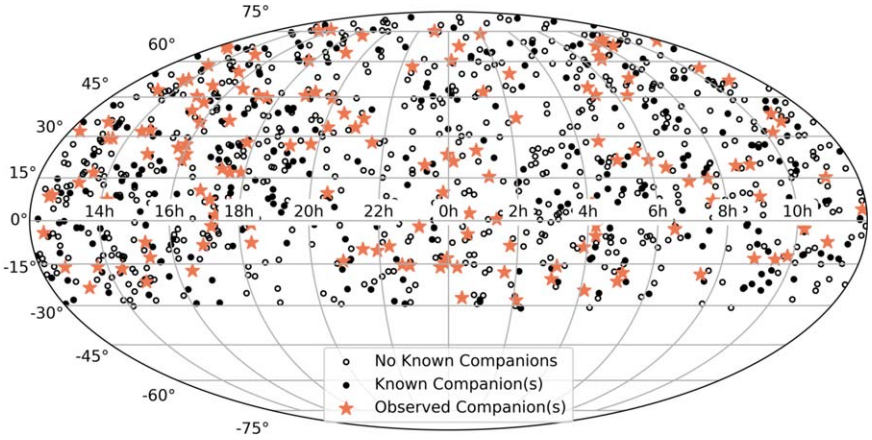

Figure 1. The sky locations of the 1125 targets in the POKEMON sample. Targets with no known companions are marked with open black circles, targets with known companions (but without companions detected by us) are marked with filled black circles, and targets with companions detected by us are marked with larger, orange stars.

Scott et al. 2018) on the 3.5 m WIYN telescope[9] at Kitt Peak National Observatory located outside Tucson, AZ. In Table 3, we list the dates of the observing runs and how many targets were observed during each run. We note that the POKEMON targets were not the only stars observed during each run; with the high cadence of speckle observations and the superior pointing of the LDT and WIYN, a hundred targets or more can easily be observed per night.

DSSI and NESSI produce diffraction-limited images from speckle patterns observed simultaneously at two wavelengths. Each instrument uses a dichroic filter to split the collimated beam from the telescope at ∼700 nm into two channels that are imaged on separate high-speed readout electron-multiplying charge-coupled devices. DSSI uses two narrowband filters centered at 692 and 880 nm, with filter widths of 40 and 50 nm, respectively. NESSI uses filters centered at 562 and 832 nm, with filter widths of 44 and 40 nm, respectively.

The raw data from DSSI and NESSI are image cubes consisting of a sequence of 1000 40 ms exposures. These short exposures are necessary to "freeze" out the atmospheric interference from the observations, and to obtain high contrast in the speckles. Bright objects ($V < 11$) require only ∼1–2 minutes of observing time, during which one data cube is acquired, while fainter targets require up to ∼10 minutes of observing time, during which up to nine data cubes are acquired. Standard observing also includes periodic observations of bright, unresolved, single stars from the Bright Star Catalog (Hoffleit & Jaschek 1982) to probe the atmospheric conditions experienced by the target of interest. All data cubes are stored as multi-extension FITS files.

The pixel scale and image orientation are empirically confirmed by observing binaries with extremely well-known orbits (those listed as Grade 1 in the Sixth Orbit Catalog; Hartkopf et al. 2001). Their ephemeris positions are computed based on the orbital elements, and their scale and orientation are derived from these results. For more information on calibration and overall speckle data quality obtainable at the LDT and WIYN, see Horch et al. (2021) and earlier papers in that series.

[9] The WIYN Observatory is a joint facility of the NSF's National Optical-Infrared Astronomy Research Laboratory, Indiana University, the University of Wisconsin-Madison, Pennsylvania State University, the University of Missouri, the University of California-Irvine, and Purdue University.

Each target was observed at least once, though some targets were observed twice, or even three or four times.

2.3. Data Reduction

The data were reduced with an updated version of the pipeline described in Horch et al. (2009, 2011a, 2011b), which uses bispectral analysis (Lohmann et al. 1983) to compute a reconstructed image from the data cube(s) collected for each target.

Multi-star systems produce fringe patterns in the Fourier plane, and we use this fact to probe the properties of each star in the system. A two-dimensional autocorrelation function is calculated for each 40 ms exposure in the data cube, and summed over all exposures. The Fourier transform of the autocorrelation function is calculated and squared in order to obtain the power spectrum, which is then normalized. After dividing by the power spectrum of a point source, the residual two-dimensional power spectrum appears as a set of fringes for each pair of stars in the field of view. The fringes are fit using a cosine-squared function to determine the relative astrometry and photometry of any pairs. The reconstructed image is constructed from the object's modulus, and the phase estimate is obtained from the bispectrum.

We note that the reconstructed images generated from our speckle observations are limited. They often contain three peaks, which derive from low signal-to-noise in the phase portion of the calculation. For our reconstructed images, we start with a "zero-phase" assumption and relax to the final phase map (Meng et al. 1990). When there is low signal-to-noise in the phase, the zero-phase assumption results in a phase map that is close to zero across the Fourier plane, resulting in a lack of phase information. The reconstructed image therefore appears similar to an inverse Fourier transform of the square root of the power spectrum. Therefore, for this work we mainly use the reconstructed images for identifying whether a star is single or multiple.

By examining annuli in the reconstructed image that are centered on the primary star, all local maxima and minima in the annulus are determined, and their mean values and standard deviations are derived. The detection limit within each annulus is estimated as the mean value of the maxima plus 5 times the average sigma of the maxima and minima. A "contrast curve" is then produced by calculating the detection limit within each

Table 1
POKEMON Targets

2MASS ID or Name	Gaia DR3 ID	G Magnitude (mag)	G_{RP} Magnitude (mag)	Distance (pc)	References	RUWE	IPDFMP	Companion(s) Detected?
00051079+4547116	386655019234959872	9.1	8.0	11.5	8	1.0	0	N
00054090+4548374	386653747925624576	8.3	7.4	11.5	8	1.2	2	N
00064325-0732147	2441630500517079808	11.8	10.4	4.8	8	1.3	4	N
00074264+6022543	429297924157113856	12.4	10.7	15.4	8	3.9	72	Y
00085391+2050252	2798766647610195456	12.0	10.7	18.1	7		8	Y
00085512+4918561	393621524910343296	14.4	13.0	14.8	8	1.1	0	N
00113182+5908400	423027104407576576	13.5	12.1	9.3	8	1.1	0	N
00152799-1608008	2368293487261055488	10.3	8.9	5.0	18		60	Y
00153905+4735220	392350008432819328	10.0	8.9	11.5	8	0.9	3	N
00154919+1333218	2768048564768256512	11.4	10.2	12.2	8	1.2	0	N

References. (1) Cifuentes et al. (2020); (2) Dittmann et al. (2014); (3) Dupuy & Liu (2017); (4) Dupuy et al. (2019); (5) Finch & Zacharias (2016); (6) Finch et al. (2018); (7) Gaia Collaboration et al. (2018); (8) Gaia Collaboration et al. (2023); (9) Gliese & Jahreiß (1991); (10) Henry et al. (2006); (11) Lépine et al. (2009); (12) Murray et al. (1986); (13) Riedel et al. (2010); (14) Torres et al. (2010); (15) van Altena et al. (1995); (16) van Leeuwen (2007); (17) Weinberger et al. (2016); (18) Winters et al. (2015); (19) Winters et al. (2017).

(This table is available in its entirety in machine-readable form.)

annulus as a function of separation (e.g., Figure 6 in Horch et al. 2011a).

We note that the contrast curves are rough estimates that can contain systematic error, particularly in the low-signal-to-noise regime as described previously. Therefore, for this work we mainly use the contrast curves to place limits on the types of companions that could still exist around "single" stars.

Two example reconstructed images and their corresponding contrast curves are shown in Figure 3. The median contrast curves from all DSSI and NESSI observations are shown in Figure 4. These contrast curves show that we typically achieve a spatial resolution of ∼40 mas, which is comparable to the resolution of the near-infrared adaptive optics system on the 10 m Keck II Telescope. Because of our achieved spatial resolution and the proximity of the POKEMON targets, we were able to identify stellar companions in the reconstructed images as close-in as ∼1 au.

3. Results

In this section, we present the companions detected throughout the POKEMON survey, as well as our evaluation of our astrometric and photometric precision.

3.1. Detected Companions

In this section, we report the observed properties for the 151 M dwarfs that had a companion detected throughout the POKEMON survey, including those from Clark et al. (2022b), Clark (2022), and Clark et al. (2023). We will present companions that are known to the literature but were not detected in our speckle images in the third paper in the series. Nonetheless, we have cross-matched the POKEMON sample with the Washington Double Star (WDS; Mason et al. 2001) catalog to guide the reader to previous epochs of observation for these multiples. Additionally, this cross-match allowed us to compare our astrometry and photometry with published values to ensure that the motion is consistent with a bound pair. This was the case for all multiples.

The properties of the detected companions are recorded in Table 4, where we have included the 2MASS ID or name of the primary, WDS ID, epoch of observation (measured in Besselian years), bandpass central wavelength (λ), bandpass width ($\Delta\lambda$), position angle (θ), angular separation (ρ), and magnitude difference (Δm). We also list the position angle, angular separation, and magnitude difference for the second companion if the system is trinary.

We note several considerations about the content of Table 4 and updates from the previous paper in the series (Clark et al. 2022b):

1. In some cases, in particular for the fainter objects, there may be a 180° ambiguity in the listed position angles due to the limitations of the reconstructed images described in Section 2.3.
2. As shown in previous LDT speckle papers (Horch et al. 2015, 2020), when the seeing value multiplied by the angular separation is larger than 0.″6 squared, then there may be a systematic error in the photometry, and the observed magnitude difference should be considered as an upper limit; i.e., the companions may be brighter than the quoted delta magnitude value. This is denoted by a < limit flag on the delta magnitude.
3. As discussed in Section 3.4, during the 2017 April observing runs, the narrowband speckle filters were not installed within DSSI. For these "filterless" observations, rather than listing the bandpass and bandpass width of the observation, we instead indicate whether the companion was detected in the $\lambda < 700$ nm image or the $\lambda > 700$ nm image. We are using these identifiers rather than the "blue" and "red" identifiers used in the previous paper in the series to avoid confusion with the UBVRI photometric system.
4. We introduce updated properties for several detections presented in the previous paper in the series.
5. In the previous paper in the series we mistakenly attributed the discovery of several companions to our own work; we note here the correct references for discoveries of these companions: 2MASS J07011725 +1348085 (El-Badry et al. 2021), 2MASS J11030845 +1517518 (Bowler et al. 2019), 2MASS J12435889-1614351 (Vrijmoet et al. 2022), 2MASS J15471513 +0149218 (Salama et al. 2021), and 2MASS J21011610 +3314328 (Cortés-Contreras et al. 2017).

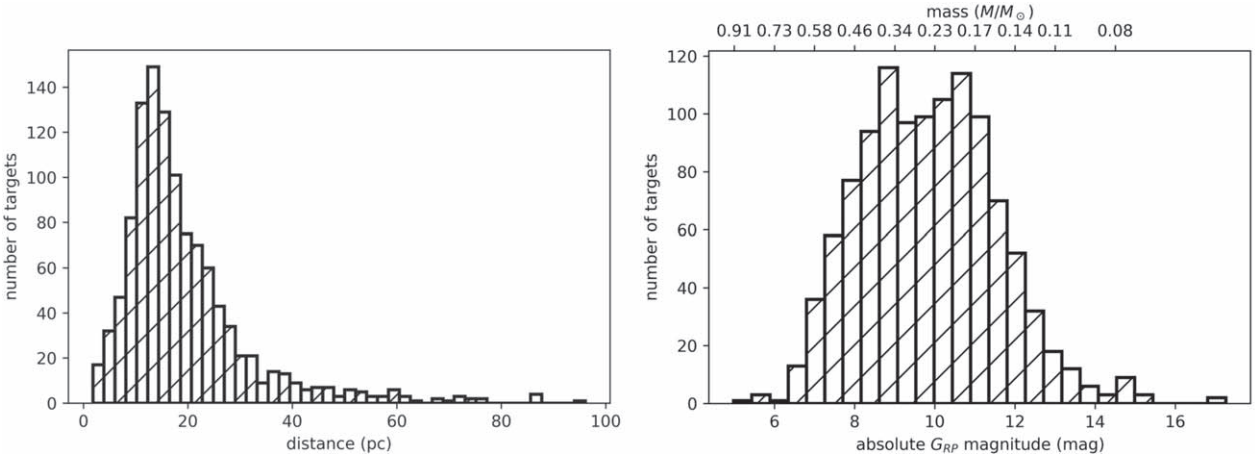

Figure 2. Distance (left) and absolute G_{RP} magnitude distributions for the 1125 targets in the POKEMON sample. Using the mass–magnitude relation from Giovinazzi & Blake (2022), we also show the estimated masses for these targets.

Table 2
Spectral Types of the Targets in the POKEMON Sample

Spectral Type	Number of Targets
K	52
M0	69
M1	77
M2	129
M3	296
M4	257
M5	203
M6	7
M7	18
M8	6
M9	1
L	8

Table 3
Observing Runs

First Night of Observing Run (UT Date)	Final Night of Observing Run (UT Date)	Instrument	Targets Observed
2017 Apr 7	2017 Apr 7	DSSI[a]	29
2017 Apr 9	2017 Apr 17	DSSI[a]	508
2017 May 4	2017 May 8	DSSI	87
2017 Oct 18	2017 Oct 18	DSSI	50
2017 Oct 20	2017 Oct 21	DSSI	127
2018 Jan 28	2018 Feb 1	DSSI	219
2018 Aug 2	2018 Aug 5	NESSI	31
2018 Aug 26	2018 Aug 26	NESSI	6
2018 Aug 26	2018 Aug 27	DSSI	32
2018 Aug 28	2018 Aug 29	NESSI	28
2018 Nov 17	2018 Nov 17	NESSI	3
2018 Nov 19	2018 Nov 22	NESSI	22
2019 Jan 18	2019 Jan 20	NESSI	15
2019 Jan 22	2019 Jan 25	NESSI	22
2019 Sep 10	2019 Sep 10	DSSI	9
2019 Sep 13	2019 Sep 14	DSSI	75
2019 Sep 16	2019 Sep 16	DSSI	2
2020 Feb 9	2020 Feb 10	DSSI	16

Note.
[a] Filterless observations.

6. We include our observations of the companions to 2MASS J10494561+3532515 and 2MASS J17335314 +1655129, but we note that the motion of the companions appears linear rather than orbital, indicating that the companions are likely unbound. This was determined using multiple published observations of 2MASS J10494561+3532515, and from unpublished adaptive optics observations of 2MASS J17335314 +1655129 (C. Gelino & D. Kirkpatrick 2023, private communication). We do not include these companions in the analysis described in Section 4.
7. As noted in the previous paper in the series, the companion we detected to the late M-dwarf 2MASS J13092185-2330350 is likely a brown dwarf, so this companion is not included in the analysis described in Section 4.
8. We later found 2MASS J14235017-1646116 to be in a common proper motion pair with a more massive M dwarf, so the new companion we reported in the previous paper in the series makes the system triple.
9. We have imaged and obtained properties for the companion to 2MASS J15411642+7559347 for the first time.

The minimum angular separation we measured was 0.″0787, and the maximum angular separation we measured was 3.″5909. The minimum delta magnitude we measured was 0 mag (at $\lambda = 880$ nm), and the maximum delta magnitude we measured that was not an upper limit was 5.21 (at $\lambda > 700$ nm). These wide ranges demonstrate the power and utility of speckle imagers to detect stellar companions, even on mid-sized (3.5 and 4.3 m) telescopes.

3.2. Astrometric Precision

To characterize our astrometric precision, we use the fact that DSSI and NESSI observe simultaneously at two wavelengths. This allows us to calculate the residuals in our astrometry by computing the difference between the observed angular separation and position angle in each channel. The angular separation residuals have an average value of 3.1 mas, with a standard deviation of 12 mas. The position angle residuals have an average value of 0.10°, with a standard deviation of 1.1°. The residuals result from the subtraction of two independent measurements with presumably the same

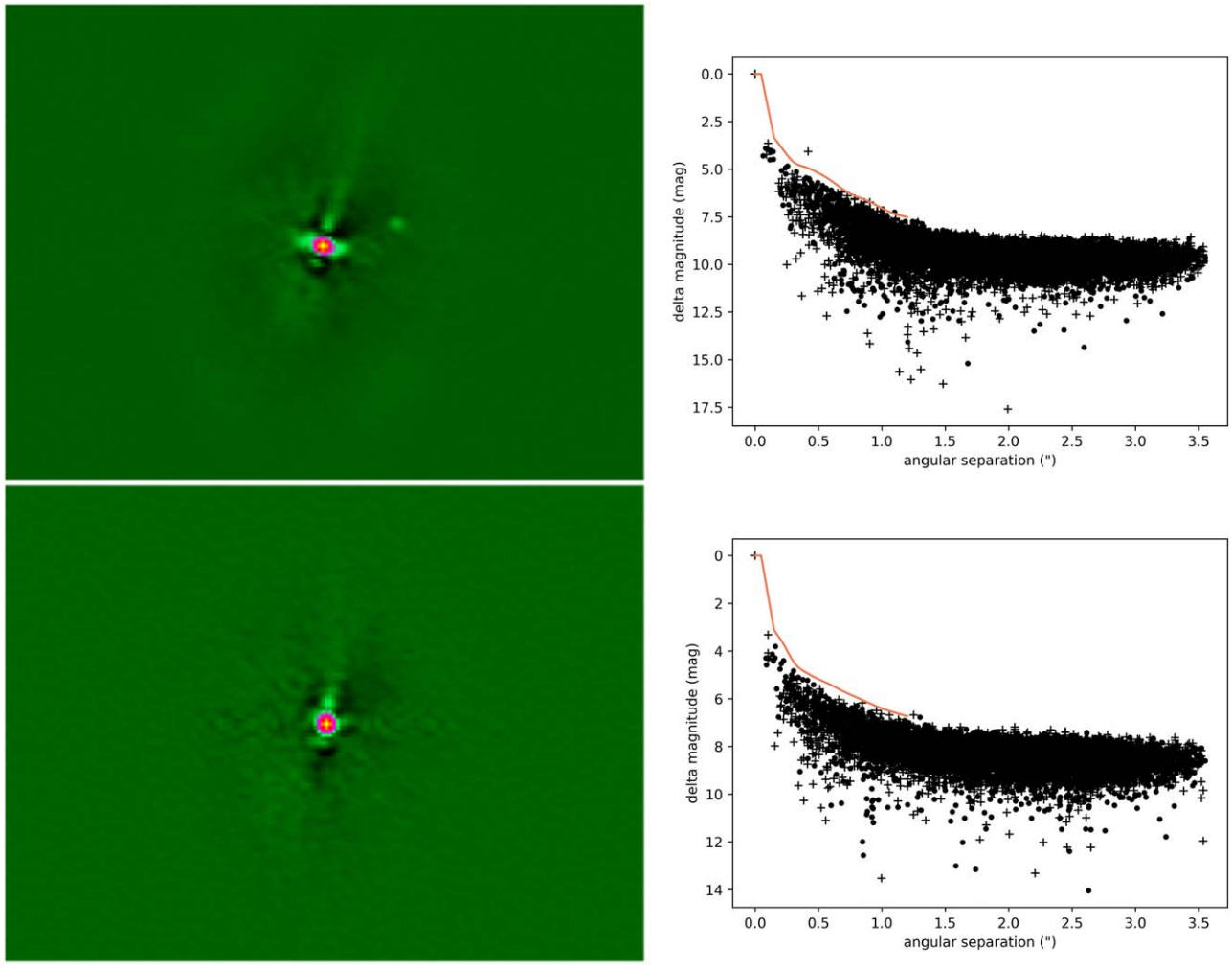

Figure 3. Top: the reconstructed image and contrast curve for 2MASS J08313759+1923395 and its companion at a separation of $0\farcs3397$ that is fainter by 5.21 mag at $\lambda > 700$ nm. This is the largest delta magnitude we measured that was not an upper limit. The companion is marked by a + sign above the contrast curve. Bottom: the reconstructed image and contrast curve for 2MASS J08294949+2646348 at $\lambda > 700$ nm. We have determined that this star is single based on the contrast limits derived from the reconstructed image.

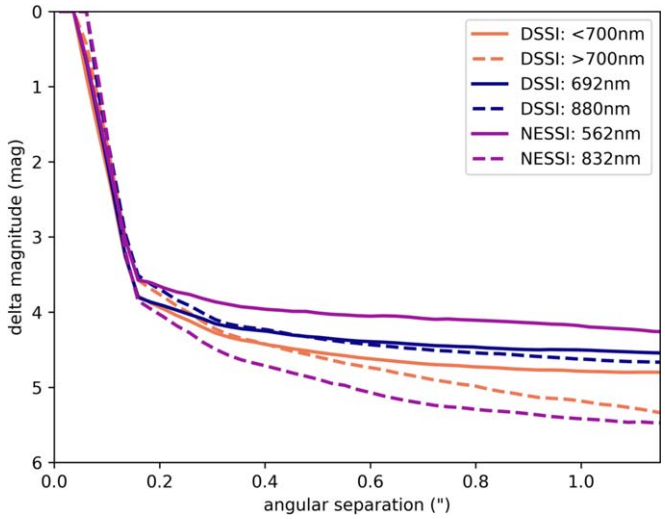

Figure 4. Median contrast curves for the <700, >700, 692, and 880 nm DSSI observations and the 562 and 832 nm NESSI observations taken throughout the POKEMON survey.

uncertainty, so the subtraction has an uncertainty that is $\sqrt{2}$ larger than the uncertainty of either individual measure. This means that the uncertainty in a single angular separation measure is given by 12 divided by $\sqrt{2}$, or 8.4 mas. The average uncertainty in position angle is then 0.77°. These values are larger than those derived in Horch et al. (2017), Colton et al. (2021), or Horch et al. (2021), which also used DSSI and NESSI; this is likely due to the faintness of our targets, and the filterless observations that took place during the 2017 April observing run. In general, filterless observations reduce the precision of our astrometry, but allow us to observe fainter companions.

In Figure 5, we investigate whether there are any trends in the difference between the observed properties in each channel as a function of the median of the angular separations obtained in the two channels. We find no trend in the angular separation residuals. In contrast, the position angle residuals increase as separation decreases, as the same positional uncertainty subtends a larger angle at small separations. If we assume that the positional uncertainty is the same as the orthogonal direction to the separation compared with the direction of

Table 4
Properties of Companions Detected throughout the POKEMON Survey

2MASS ID or Name	WDS ID	Epoch (2000+)	λ (nm)	$\Delta\lambda$ (nm)	θ_1 (°)	ρ_1 (″)	Δm_1 (mag)	θ_2 (°)	ρ_2 (″)	Δm_2 (mag)
00074264+6022543	00077+6022	18.5887	562	44	107.6	0.9750	0.95			
		18.5887	832	40	107.9	0.9774	0.76			
00085391+2050252	00089+2050	18.5853	832	40	232.4	0.1329	0.64			
00152799-1608008	00155-1608	17.8025	692	40	131.6	0.1944	2.46			
		17.8025	880	50	131.1	0.1910	1.64			
		18.6571	832	40	4.8	0.2146	1.58			
00244419-2708242	00247-2653	18.6571	832	40	51.7	0.9122	<2.41			
00322970+6714080	00321+6715	18.5887	562	44	354.7	0.4695	3.94	185.4	3.5795	<2.78
		18.5887	832	40	355.3	0.4806	3.05	185.6	3.5909	<2.46
		19.0643	832	40	3.8	0.4941	2.44			

Note. Astrometric and photometric uncertainties are described in Sections 3.2 and 3.3, respectively.

(This table is available in its entirety in machine-readable form.)

separation itself, then we would expect the scatter in the position angle to vary as

$$\delta\theta = \arctan\left(\frac{\delta\rho}{\rho}\right) = \arctan\left(\frac{8.4\text{ mas}}{\rho}\right), \quad (1)$$

where $\delta\theta$ is the uncertainty in the position angle difference and $\delta\rho$ is the uncertainty in the angular separation difference. We do find that the scatter in position angle as a function of angular separation is consistent with these values.

Figure 5 also shows the angular separation and position angle differences as a function of the median of the delta magnitudes obtained in the two channels; however, we do not see a trend in either of these cases. We conclude that there are no identifiable sources of systematic error in the data set.

3.3. Photometric Precision

In order to assess our photometric precision, we compare the magnitude differences derived from our speckle images to magnitude differences from Gaia DR3. The Gaia G and R_p filters are reasonably similar to the 562 and 692 nm filters used throughout this survey. However, many of the companions we observed were only detected at 832 or 880 nm. Additionally, as discussed in Section 4.1, many stellar multiples with angular separations less than $\sim$1″—the vast majority of our detected multiples—are unresolved in Gaia, and often do not have astrometric or photometric solutions. Taking these limitations into account, we are left with 51 observations to use for our photometric analysis.

We show a comparison between the Gaia and speckle magnitude differences in Figure 6. We first plot the difference between the speckle magnitude difference and the Gaia magnitude difference as a function of seeing times separation, which can be used as a way to judge the isoplanicity of the observations and thus the reliability of the photometry. The larger this quantity is, the less the speckle patterns of the primary and secondary resemble one another, causing the secondary to appear fainter than it really is. The difference between the speckle and Gaia magnitude differences should be $\sim$0 for small values of seeing times separation, and should increase as seeing times separation increases. This is the trend we see in our data.

We also plot Gaia magnitude difference versus speckle magnitude difference for the 15 observations where seeing times separation is <0.6 arcsec^2, which should be relatively unaffected by nonisoplanicity, and should therefore correlate well with the Gaia magnitude difference values. The correlation is fairly good, although it does appear that there is a systematic offset from an equivalent relation. The residuals from these magnitude differences have an average value of 0.25 mag, with a standard deviation of 0.54 mag. We divide by $\sqrt{2}$, so the average uncertainty in magnitude difference is 0.38.

3.4. Filtered versus Filterless Observations

During our 2017 April observing run, the narrowband speckle filters were not installed within DSSI, so the beam was simply split at $\lambda \sim 700$ nm. When observing without narrowband filters, more photons reach the detectors, resulting in additional sensitivity to faint stellar companions. However, there is also less contrast in the speckles, and significant chromatic effects arise at high airmass. Therefore, for all other observing runs, the narrowband speckle filters were used within DSSI.

Now that all observing runs are complete, we investigate whether there were any systematic effects in our data either from ambient conditions or target brightness during both the filtered and the filterless observing runs. Figure 4 shows an increase in our limiting magnitude of $\sim$0.5 mag when the speckle filters are not used. If there are no systematic effects in the filterless data, then these results indicate that filterless observations may provide better detection performance than filtered observations.

We find that the ambient conditions were comparable between the filterless observing runs and all other observing runs, although the seeing was slightly better during the filterless observing run, with a median value of 0.79 ($\sigma = 0.3$) as compared to a median value of 0.90 ($\sigma = 0.4$) for the filtered observing runs.

We also find that the target brightnesses were comparable between the filterless and filtered observing runs. If anything, the targets observed during the filterless observing run were a bit fainter, with a median G magnitude of 12.1 ($\sigma = 1.9$). The targets observed during the filtered observing runs had a median G magnitude of 11.8 ($\sigma = 1.6$).

Overall, 27 systems were observed both with and without the speckle filters installed. As there do not appear to be any major systematic effects that disfavor the filtered observations, we conclude that the filterless observations may provide better

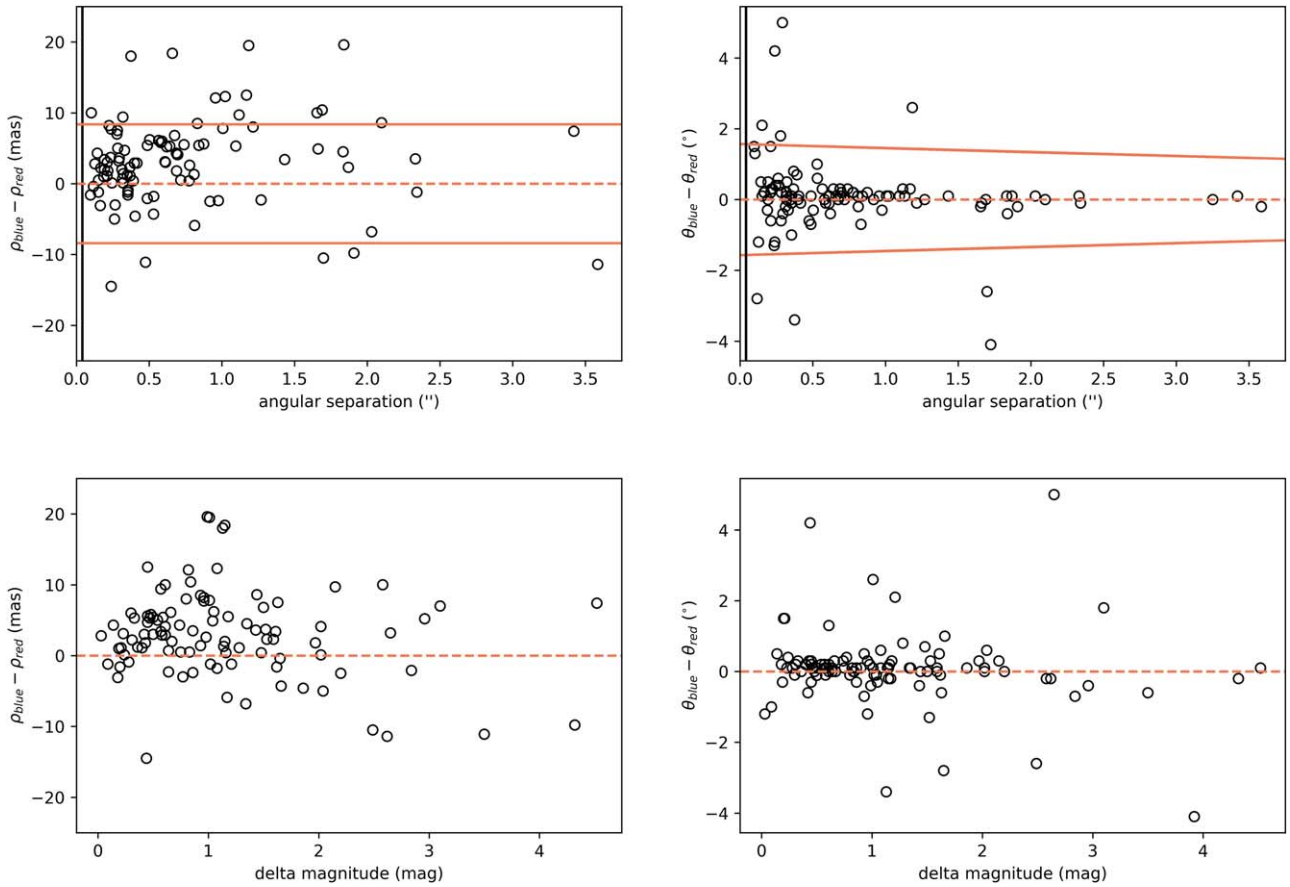

Figure 5. Top: differences in angular separation and position angle as a function of angular separation. In both plots, a dashed orange line at a difference of zero is shown to guide the eye, and the solid orange lines indicate the $\pm 1\sigma$ in estimated internal repeatability of individual measures as a function of angular separation. For differences in separation, this value is the standard deviation of the measures, and for position angle this value is proportional to arctan $\left(\frac{\delta\rho}{\rho}\right)$. The solid black line indicates the formal diffraction limit of the LDT. Bottom: differences in angular separation and position angle as a function of delta magnitude. A dashed orange line at a difference of zero is shown to guide the eye.

detection performance than filtered observations in future observing runs.

4. Discussion

In this section, we evaluate the effect of stellar multiplicity on Gaia astrometry and assess any potentially missed companions.

4.1. Evaluating the Effect of Stellar Multiplicity on Gaia Astrometry

The long-term astrometric monitoring from Gaia (Gaia Collaboration et al. 2016, 2018, 2021, 2023) has proven invaluable for diverse science cases such as stellar variability, the structure of the solar neighborhood and the Milky Way as a whole, and, in the future, even exoplanet detection. However, in the currently available Gaia data releases, the relative motion of close-in binary systems disrupts the ability of Gaia to provide astrometric solutions for the components. This will not be the case for future Gaia data releases, as the solutions included in these data releases will use astrometric data collected over longer time baselines, and perhaps improved analysis. In the meantime, we attempt to quantify the extent to which close-in multiples affect Gaia astrometry, and show the utility of using high-resolution speckle observations to supplement and complement Gaia data.

In Figure 7, we plot the 151 POKEMON targets with companions detected throughout the POKEMON survey. We have evaluated whether these companions were resolved in Gaia DR3, and whether there was an astrometric solution for the primary and for the companion. We find that the majority (58.9%) of the companions we detected in our speckle images were *not* resolved in Gaia, demonstrating the need for high-resolution imaging in addition to long-term astrometric monitoring. In general, the companions that were not resolved by Gaia were within 1″ and had large delta magnitudes.

However, multiple Gaia parameters are known to indicate the presence of a stellar companion. First, the Gaia RUWE acts like a reduced chi-squared, where large values can indicate a poor model fit to the astrometry, assuming that the star is single. Single sources typically have RUWE values of $\sim$1, while sources with RUWE values $>$1.4 are likely nonsingle or otherwise extended (Ziegler et al. 2020; Gaia Collaboration et al. 2021). Following Vrijmoet et al. (2020), which surveyed M dwarfs specifically, we use RUWE > 2 to distinguish single and (potentially) nonsingle sources. Additionally, the IPDFMP value provides the fraction of windows—as a percentage from 0 to 100—for which the image parameter determination (IPD) algorithm has identified a double peak, meaning that the

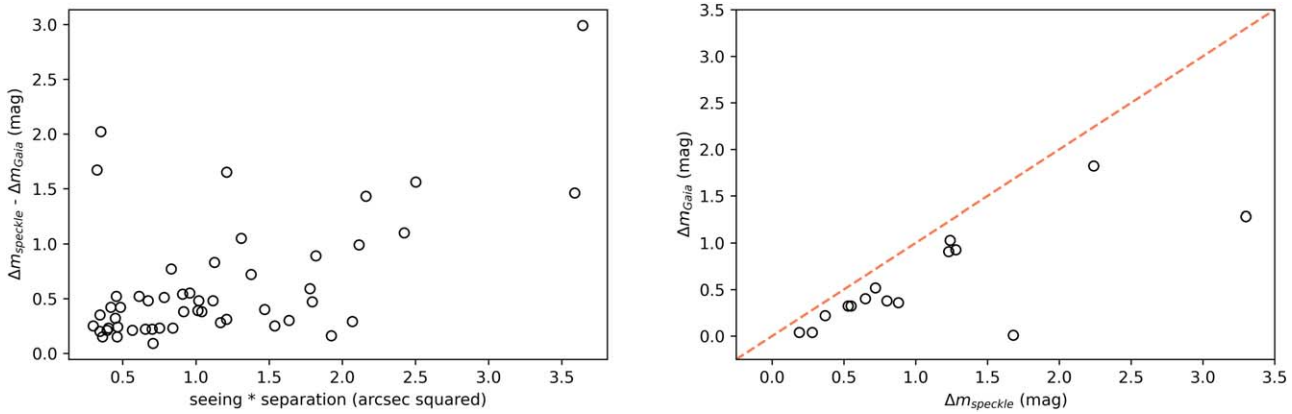

Figure 6. Left: difference between speckle magnitude difference and Gaia magnitude difference as function of seeing times separation. This difference between the speckle and Gaia magnitude differences should be ∼0 for small values of seeing times separation, and should increase as seeing times separation increases. This is the trend we see in our data. Right: Gaia magnitude difference vs. speckle magnitude difference for the observations where seeing times separation is <0.6 arcsec^2. The correlation is fairly good, although it does appear that there is a systematic offset from an equivalent relation (dashed orange line).

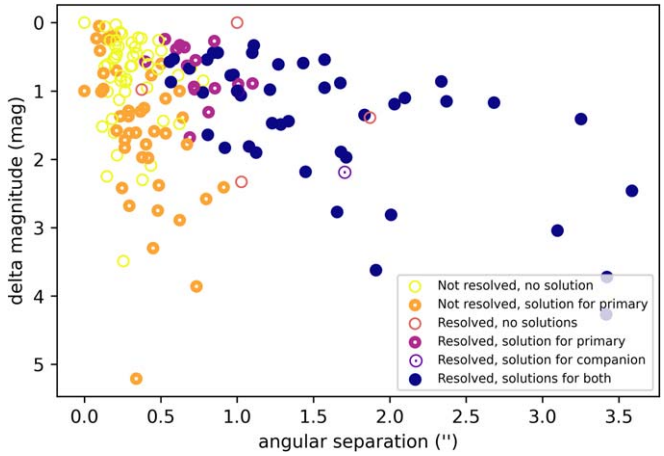

Figure 7. Scatter plot of median *I*-band delta magnitude vs. median angular separation for the 151 POKEMON targets with companions detected throughout the POKEMON survey. The different points represent whether the multiple was resolved in Gaia DR3, and whether there was an astrometric solution for the primary and for the companion. The majority (58.9%) of the companions we detected in our speckle images were *not* resolved in Gaia, demonstrating the need for high-resolution imaging in addition to long-term astrometric monitoring.

detection may be a visually resolved double star. Following Tokovinin (2023), we use IPDFMP > 2 to distinguish single and (potentially) nonsingle sources.

In order to understand how often a high RUWE or IPDFMP value indicates the presence of an unseen companion, we plot the RUWE and IPDFMP values as a function of angular separation for the 41 POKEMON multiples that were not resolved in Gaia DR3, but with a Gaia DR3 astrometic solution in Figure 8 (48 unresolved POKEMON multiples did not have Gaia DR3 astrometric solutions). We find that all of the unresolved companions whose primaries have Gaia DR3 astrometric solutions are within 1″. While the RUWE and IPDFMP values do not reveal the presence of an unseen companion in every case, we do find that the majority (78.0%) of the RUWE values are greater than 2, and that the median RUWE value is 9.1. We find that 82.9% of the IPDFMP values are greater than 2, and that the median IPDFMP value is 51. These results indicate that, even though Gaia astrometry can become unreliable for close-in stellar multiples, the RUWE and IPDFMP values can still be a useful identifier of potential unseen stellar companions. However, these results also indicate that high-resolution imaging—in addition to long-term astrometric monitoring from Gaia—is critical for both resolving stellar multiples and determining the properties of any unseen companions.

Table 5
Potential Multiples

2MASS ID	RUWE	IPDFMP
06043887+0741545	3.1	63
06170531+8353354	17.0	76
08115757+0846220	2.1	4
08505062+5253462	5.4	67
08255285+6902016	4.6	53
08561768-2326574	2.9	98
11065691-1244024	8.9	3
12394672+0410471	3.2	21
13525004+6537197	2.4	73
14442602-1800065	14.4	82
20125995+0112584	7.9	4
23373831-1250277	6.6	12

We also investigated whether any of the stars we have deemed single have elevated RUWE and IPDFMP values, indicating that they may have an as-yet undetected stellar companion. We find that 12 of the "single" stars in our sample have both RUWE and IPDFMP values over 2; we list these targets Table 5. These stars are potential targets for additional high-resolution and/or high-contrast imaging, or spectroscopic follow-up.

4.2. Assessing Potentially Missed Companions

In order to identify the population of stellar companions that were not detected in our speckle images—such as those indicated by a lack of a Gaia astrometric solution or a high RUWE value—we used existing code that was originally developed for Palomar and Keck adaptive optics observations (Lund & Ciardi 2020) and adapted it to the specific needs of the POKEMON survey and our speckle observations. The purpose of these simulations is to estimate the fraction of stellar

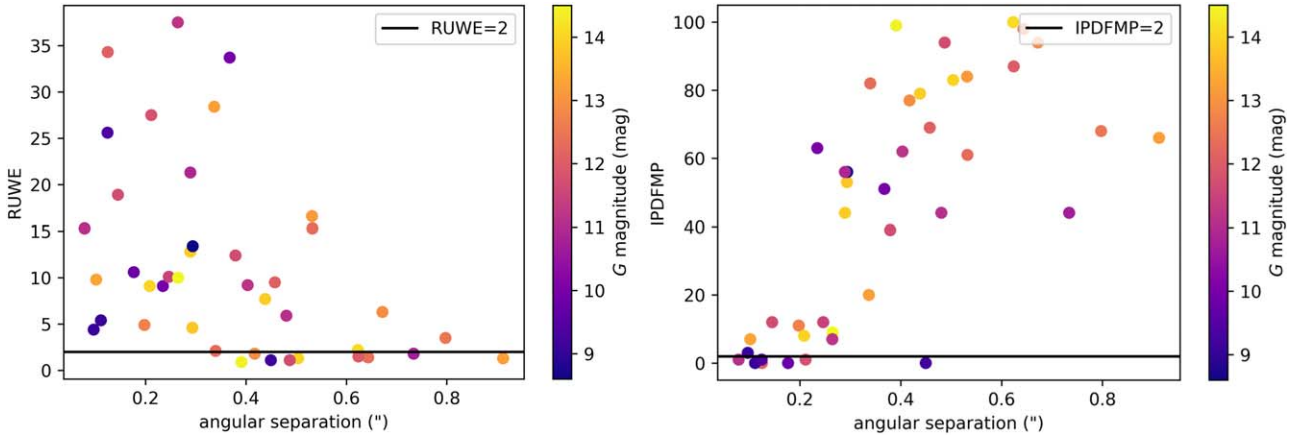

Figure 8. Scatter plot of Gaia RUWE value (left) and IPDFMP value (right) vs. angular separation for the 41 POKEMON multiples that were not resolved in Gaia DR3, but for which the primary has a Gaia DR3 astrometric solution. The points are color-coded by Gaia *G* magnitude, and the black line indicates a RUWE value of 2. All of the unresolved multiples are within 1″. While the RUWE does not reveal the presence of an unseen companion in every case, we do find that the majority (78.0% and 82.9%, respectively) of the RUWE and IPDFMP values are greater than 2, and that the median RUWE and IPDFMP values are 9.1 and 51, respectively. These results indicate that the RUWE and IPDFMP value can be useful identifiers of unseen stellar companions. In particular, the RUWE value is useful for close-in multiples, and the IPDFMP value is useful for wider multiples. However, these results also indicate that high-resolution imaging—in addition to long-term astrometric monitoring from Gaia—is critical for both resolving stellar multiples and determining the properties of any unseen companions.

companions that would be detectable within our speckle images, assuming that the star has a companion.

The code works by first identifying the population of stellar companions that could orbit each star, and then uses the derived contrast curves to evaluate the sensitivity of each observation to these stellar companions. Specifically, the code identifies the populations of stellar companions by matching the star to a best-fit stellar isochrone from the Dartmouth isochrones (Dotter et al. 2008). The primary goal of the isochrone fitting is to estimate the stellar mass range that may have been missed by the high-resolution imaging. Given that the majority of the POKEMON targets do not have age estimates, the age of the primary star is not set a priori, and the isochrone fitting is done across all of the possible Dartmouth models (0.25–15 Gyr). The fitting yielded stellar ages that are consistent with the M-dwarf main sequence, but that were not actually used to age the stars. Given the long lifetime of the M dwarfs, uncertainties in the isochrone fitting due to age are dwarfed by the general uncertainties in the photometric fitting, so the isochrone fitting yields reasonable estimates of the mass range that remained undetected. See Figure 9 for additional discussion of the isochrone fitting.

The code then independently draws from the mass ratio and orbital period distributions for M dwarfs from the Duchêne & Kraus (2013) review paper on stellar multiplicity. The code makes the assumption that if the companion is outside the field of view of the instrument, then it would be revealed by other methods. We also account for any known companions (when their properties are available), as they could influence the population of stellar companions that could orbit their host star.

An example of the simulated companions is shown in Figure 10. The separations for the simulated companions are calculated assuming a circular orbit, and using the period and stellar masses to compute a semimajor axis. The companion is then given a random position on that orbit. This simulation is performed 10,000 times for each star. These simulations allow us to determine the fraction of stellar companions that would be detectable within our speckle images.

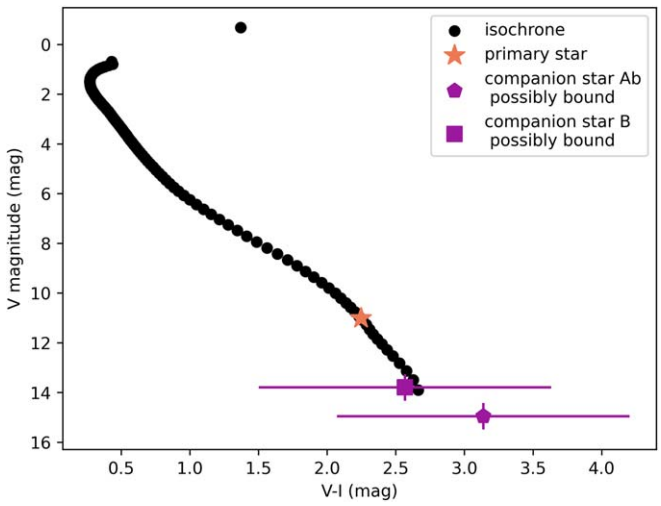

Figure 9. Example of the isochrone fitting carried out to estimate the stellar mass range that may have been missed by our high-resolution imaging. This color–magnitude diagram corresponds to 2MASS J00322970+6714080, and the plotted isochrone corresponds to an age of 0.9 Gyr. The distance to this object is 10 pc, so here the apparent and absolute magnitudes are identical. However, it should be noted that if the companions are unbound stars at an arbitrary distance, then they may be far from the isochrone that fits the primary in absolute magnitude space. Nonetheless, the fact that the companions are self-consistently compatible with having the same distance as the primary still has informational value. While color uncertainties of the secondary and tertiary components in this system are still large at this point, the placement of these objects on the color–magnitude diagram is consistent with a gravitationally bound triple system.

We note that 70 of the 1125 POKEMON targets were unable to be included in the Lund & Ciardi (2020) analysis, either because their mass was too low to be fit with a Dartmouth isochrone, because their mass was too low to simulate a meaningful number of potential stellar companions, or because we were unable to determine a mass or distance for the target. Nonetheless, we were able to carry out this analysis on 93.8% of the targets in the POKEMON sample. For these targets, we find that the majority of potential stellar companions would be

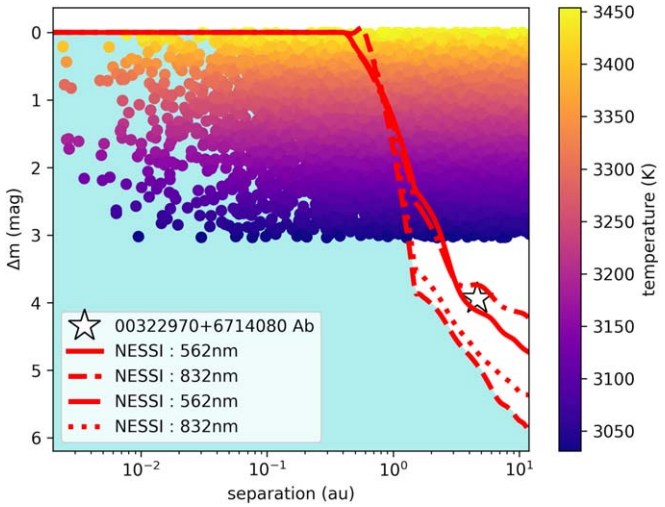

Figure 10. Simulated companions and derived contrast curves for the triple system 2MASS J00322970+6714080. For this particular star, 76.5% of the simulated stellar companions would be detectable within our speckle images, and we did indeed detect both companions. The inner companion to this star is shown here near the limits of the contrast curves.

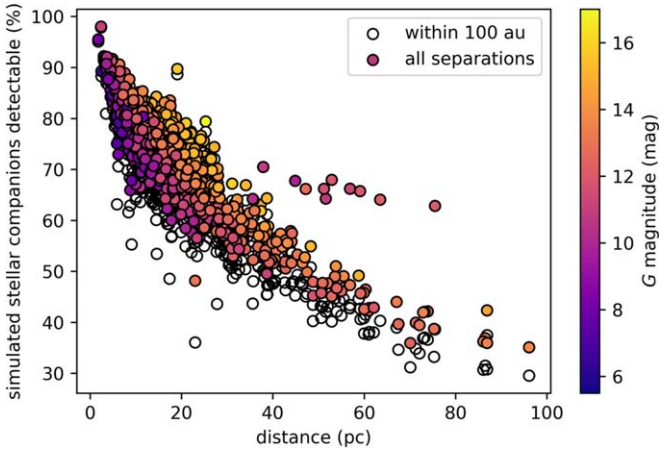

Figure 11. Percent of stellar companions detectable within our speckle images vs. distance. Circles color-coded by *G* magnitude represent the detectability of simulated companions at all separations. Open black circles represent the detectability of simulated companions specifically within 100 au. We find that the majority of potential stellar companions would be detectable, particularly for the nearby targets, with a median value of 73.2%. Specifically, within 100 au we find that 70.3% of simulated companions are recovered.

detectable by our speckle observations, particularly for the nearby targets (Figure 11); we find a median value of 73.2%. Specifically, within 100 au we find that 70.3% of simulated companions are recovered. In general, the simulated companions that were not detected by our technique are either very close-in, or are much fainter than their primary stars.

We note that neither the Dartmouth isochrones nor the Duchêne & Kraus (2013) distributions are perfect for simulating companions to the POKEMON sample, as the Dartmouth isochrones only go through M6V, and the Duchêne & Kraus (2013) have a lower limit for the primary star at 0.1 $M_{\odot}$. In addition, as described previously, we consider our speckle photometry approximate. Nonetheless, we deem these resources the most appropriate to assess the completeness of our observations based on what is currently available in the literature. However, these biases do point to the necessity of a comprehensive M-dwarf multiplicity survey that examines the distributions of stellar companions to M dwarfs at all mass ratios and orbital periods. Ongoing work that will be presented in a future paper in the series will provide these updated mass ratio and orbital period distributions; this work is discussed further in Section 5.

5. Conclusions and Future Work

We have carried out the POKEMON speckle survey of nearby M dwarfs using the DSSI and NESSI instruments on the 4.3 m LDT and the 3.5 m WIYN telescope, respectively. Using these instruments, we imaged 1125 targets, and have revealed companions to 151 of them.

We evaluate our astrometric and photometric precision, and compare our filtered and filterless speckle observations.

We investigate the effect of this stellar multiplicity on Gaia astrometry, and find that the majority (58.9%) of the companions we detect in our speckle images were *not* resolved in Gaia, demonstrating the need for high-resolution imaging in addition to long-term astrometric monitoring. We do, however, argue that the Gaia RUWE and IPDFMP values can be a useful tool for assessing the likelihood of an unseen stellar companion, and we note 14 potentially multiple systems identified via these metrics.

We also find that the majority (73.2%) of simulated stellar companions would be detectable by our speckle observations, particularly for the nearby targets. Specifically, within 100 au we find that 70.3% of simulated companions are recovered.

We are continuing to follow up the POKEMON targets with the Quad-camera Wave front-sensing Six-channel Speckle Interferometer (Clark et al. 2020). Additionally, upcoming POKEMON papers will present the stellar multiplicity rate of M dwarfs within 15 pc (C. A. Clark et al. 2024, in preparation), as well as the stellar multiplicity rate of M dwarfs within 15 pc calculated by spectral subtype through M9V for the first time.

Acknowledgments

We thank the anonymous reviewer, J. Davy Kirkpatrick, Chris Gelino, Alex Polanski, Mark Popinchalk, and Frederick Hahne for their insightful contributions to this manuscript. We are also thankful to the army of TOs at the LDT and the WIYN Telescope for all of their assistance during our 50 nights of observing.

This research was carried out at the Jet Propulsion Laboratory, California Institute of Technology, under a contract with the National Aeronautics and Space Administration (grant No. 80NM0018D0004). This research was supported by NSF grant No. AST-1616084 awarded to G.T.v.B. and NASA grant No. 18-2XRP18_2-0007 awarded to DRC.

These results made use of the Lowell Discovery Telescope at Lowell Observatory. Lowell is a private, nonprofit institution dedicated to astrophysical research and public appreciation of astronomy and operates the LDT in partnership with Boston University, the University of Maryland, the University of Toledo, Northern Arizona University, and Yale University. Lowell Observatory sits at the base of mountains sacred to tribes throughout the region. We honor their past, present, and future generations, who have lived here for millennia and will forever call this place home.

These results are also based on observations from Kitt Peak National Observatory, the NSF's National Optical-Infrared

Astronomy Research Laboratory (NOIRLab Prop. ID: 2018B-0126; PI: C. Clark), which is operated by the Association of Universities for Research in Astronomy (AURA) under a cooperative agreement with the National Science Foundation. The authors are honored to be permitted to conduct astronomical research on Iolkam Du'ag (Kitt Peak), a mountain with particular significance to the Tohono O'odham. Data presented herein were obtained at the WIYN Observatory from telescope time allocated to NN-EXPLORE through the scientific partnership of the National Aeronautics and Space Administration, the National Science Foundation, and the NSF's National Optical-Infrared Astronomy Research Laboratory. Observations in the paper made use of the NN-EXPLORE Exoplanet and Stellar Speckle Imager (NESSI). NESSI was funded by the NASA Exoplanet Exploration Program and the NASA Ames Research Center. NESSI was built at the Ames Research Center by Steve B. Howell, Nic Scott, Elliott P. Horch, and Emmett Quigley.

This work presents results from the European Space Agency (ESA) space mission. Gaia data are being processed by the Gaia Data Processing and Analysis Consortium (DPAC). Funding for the DPAC is provided by national institutions, in particular the institutions participating in the Gaia MultiLateral Agreement (MLA). The Gaia mission website is https://cosmos.esa.int/gaia. The Gaia archive website is https://archives.esac.esa.int/gaia.

This work has used data products from the Two Micron All Sky Survey (Skrutskie et al. 2019), which is a joint project of the University of Massachusetts and the Infrared Processing and Analysis Center at the California Institute of Technology, funded by NASA and NSF.

This research has made use of the Exoplanet Follow-up Observation Program (ExoFOP, DOI:10.26134/ExoFOP5) website, which is operated by the California Institute of Technology, under contract with the National Aeronautics and Space Administration under the Exoplanet Exploration Program.

Information was collected from several additional large database efforts: the Simbad database and the VizieR catalog access tool, operated at CDS, Strasbourg, France; NASA's Astrophysics Data System; and the Washington Double Star Catalog maintained at the US Naval Observatory.

Facilities: LDT(DSSI), WIYN(NESSI).

Software: Astropy (Astropy Collaboration et al. 2013), Astroquery (Ginsburg et al. 2019), IPython (Pérez & Granger 2007), Matplotlib (Hunter 2007), NumPy (Harris et al. 2020), Pandas (McKinney et al. 2010), SciPy (Virtanen et al. 2020).

ORCID iDs

Catherine A. Clark https://orcid.org/0000-0002-2361-5812
Gerard T. van Belle https://orcid.org/0000-0002-8552-158X
Elliott P. Horch https://orcid.org/0000-0003-2159-1463
Michael B. Lund https://orcid.org/0000-0003-2527-1598
David R. Ciardi https://orcid.org/0000-0002-5741-3047
Kaspar von Braun https://orcid.org/0000-0002-5823-4630
Jennifer G. Winters https://orcid.org/0000-0001-6031-9513
Mark E. Everett https://orcid.org/0000-0002-0885-7215
Zachary D. Hartman https://orcid.org/0000-0003-4236-6927
Joe Llama https://orcid.org/0000-0003-4450-0368

References

Alonso-Floriano, F. J., Morales, J. C., Caballero, J. A., et al. 2015, A&A, 577, A128
Astropy Collaboration, Robitaille, T. P., Tollerud, E. J., et al. 2013, A&A, 558, A33, E. J.
Baraffe, I., & Chabrier, G. 1996, ApJL, 461, L51
Bowler, B. P., Hinkley, S., Ziegler, C., et al. 2019, ApJ, 877, 60
Ciardi, D. R., Beichman, C. A., Horch, E. P., & Howell, S. B. 2015, ApJ, 805, 16
Cifuentes, C. 2023, PhD thesis, Complutense University of Madrid, Spain
Cifuentes, C., Caballero, J. A., Cortés-Contreras, M., et al. 2020, A&A, 642, A115
Clark, C. A. 2022, RNAAS, 6, 242
Clark, C. A., Horch, E. P., & Davidson, J. W. 2023, RNAAS, 7, 206
Clark, C. A., van Belle, G. T., Ciardi, D. R., et al. 2022a, AJ, 163, 232
Clark, C. A., van Belle, G. T., Horch, E. P., et al. 2020, Proc. SPIE, 11446, 114462A
Clark, C. A., van Belle, G. T., Horch, E. P., et al. 2022b, AJ, 164, 33
Colton, N. M., Horch, E. P., Everett, M. E., et al. 2021, AJ, 161, 21
Cortés-Contreras, M., Béjar, V. J. S., Caballero, J. A., et al. 2017, A&A, 597, A47
Deshpande, R., Blake, C. H., Bender, C. F., et al. 2013, AJ, 146, 156
Dittmann, J. A., Irwin, J. M., Charbonneau, D., & Berta-Thompson, Z. K. 2014, ApJ, 784, 156
Dotter, A., Chaboyer, B., Jevremović, D., et al. 2008, ApJS, 178, 89
Dressing, C. D., & Charbonneau, D. 2015, ApJ, 807, 45
Duchêne, G., & Kraus, A. 2013, ARA&A, 51, 269
Dupuy, T. J., & Liu, M. C. 2012, ApJS, 201, 19
Dupuy, T. J., & Liu, M. C. 2017, ApJS, 231, 15
Dupuy, T. J., Liu, M. C., Best, W. M. J., et al. 2019, AJ, 158, 174
El-Badry, K., Rix, H.-W., & Heintz, T. M. 2021, MNRAS, 506, 2269
Finch, C. T., & Zacharias, N. 2016, AJ, 151, 160
Finch, C. T., Zacharias, N., & Jao, W.-C. 2018, AJ, 155, 176
Gaia Collaboration, Brown, A. G. A., Vallenari, A., et al. 2018, A&A, 616, A1
Gaia Collaboration, Brown, A. G. A., Vallenari, A., et al. 2021, A&A, 649, A1
Gaia Collaboration, Prusti, T., de Bruijne, J. H. J., et al. 2016, A&A, 595, A1
Gaia Collaboration, Vallenari, A., Brown, A. G. A., et al. 2023, A&A, 674, A1
Ginsburg, A., Sipőcz, B. M., Brasseur, C. E., et al. 2019, AJ, 157, 98
Giovinazzi, M. R., & Blake, C. H. 2022, AJ, 164, 164
Gliese, W., & Jahreiß, H. 1991, in Preliminary Version of the Third Catalogue of Nearby Stars, On: The Astronomical Data Center CD-ROM: Selected Astronomical Catalogs, ed. L. E. Brotzmann & S. E. Gesser, Vol. I (Greenbelt, MD: NASA/Astronomical Data Center, Goddard Space Flight Center)
Haghighipour, N., & Raymond, S. N. 2007, ApJ, 666, 436
Harris, C. R., Millman, K. J., van der Walt, S. J., et al. 2020, Natur, 585, 357
Hartkopf, W. I., Mason, B. D., & Worley, C. E. 2001, AJ, 122, 3472
Henry, T. J. 1991, PhD thesis, University of Arizona
Henry, T. J., Jao, W.-C., Subasavage, J. P., et al. 2006, AJ, 132, 2360
Henry, T. J., Jao, W.-C., Winters, J. G., et al. 2018, AJ, 155, 265
Hoffleit, D., & Jaschek, C. 1982, The Bright Star Catalogue. Fourth Revised Edition. (Containing Data Compiled through 1979) (New Haven, CT: Yale Univ. Obs.)
Horch, E. P., Broderick, K. G., Casetti-Dinescu, D. I., et al. 2021, AJ, 161, 295
Horch, E. P., Casetti-Dinescu, D. I., Camarata, M. A., et al. 2017, AJ, 153, 212
Horch, E. P., Gomez, S. C., Sherry, W. H., et al. 2011a, AJ, 141, 45
Horch, E. P., van Altena, W. F., Howell, S. B., Sherry, W. H., & Ciardi, D. R. 2011b, AJ, 141, 180
Horch, E. P., van Belle, G. T., Davidson, J. W. J., et al. 2015, AJ, 150, 151
Horch, E. P., van Belle, G. T., Davidson, J. W. J., et al. 2020, AJ, 159, 233
Horch, E. P., Veillette, D. R., Baena Gallé, R., et al. 2009, AJ, 137, 5057
Howell, S. B., Matson, R. A., Ciardi, D. R., et al. 2021, AJ, 161, 164
Hunter, J. D. 2007, CSE, 9, 90
Iben, I. J. 1991, ApJS, 76, 55
Jang-Condell, H. 2015, ApJ, 799, 147
Janson, M., Hormuth, F., Bergfors, C., et al. 2012, ApJ, 754, 44
Jódar, E., Pérez-Garrido, A., Díaz-Sánchez, A., et al. 2013, MNRAS, 429, 859
Kirkpatrick, J. D., Schneider, A., Fajardo-Acosta, S., et al. 2014, ApJ, 783, 122
Lada, E. A., Depoy, D. L., Evans, N. J. I., & Gatley, I. 1991, ApJ, 371, 171
Laughlin, Gregory, Bodenheimer, Peter, & Adams, Fred C. 1997, ApJ, 482, 420
Law, N. M., Hodgkin, S. T., & Mackay, C. D. 2008, MNRAS, 384, 150
Lépine, S., Thorstensen, J. R., Shara, M. M., & Rich, R. M. 2009, AJ, 137, 4109

Levine, S. E., Ellsworth-Bowers, T., Bida, T. A., Hamilton, R., & Kuehn, K. 2022, Proc. SPIE, 12182, 1218227
Lohmann, A. W., Weigelt, G., & Wirnitzer, B. 1983, ApOpt, 22, 4028
Luhman, K. L., & Sheppard, S. S. 2014, ApJ, 787, 126
Lund, M. B., & Ciardi, D. 2020, AAS Meeting Abstracts, 235, 249.06
Magnier, E. A., Liu, M. C., Aller, K., Best, W., & Deacon, N. 2015, IAUGA, 29, 2257922
Mason, Brian D., Wycoff, Gary L., Hartkopf, William I., Douglass, Geoffrey G., & Worley, Charles E. 2001, AJ, 122, 3466
Mason, B. D., Hartkopf, W. I., Gies, D. R., Henry, T. J., & Helsel, J. W. 2009, AJ, 137, 3358
Mason, B. D., Henry, T. J., Hartkopf, W. I., ten Brummelaar, T., & Soderblom, D. R. 1998, AJ, 116, 2975
McKinney, W. 2010, in Proc. 9th Python in Science, ed. S van der Walt & J Millman (Austin, TX: SciPy), 51
Meng, J., Aitken, G. J. M., Hege, E. K., & Morgan, J. S. 1990, JOSAA, 7, 1243
Murray, C. A., Argyle, R. W., & Corben, P. M. 1986, MNRAS, 223, 629
Pecaut, M. J., & Mamajek, E. E. 2013, ApJS, 208, 9
Pérez, F., & Granger, B. E. 2007, CSE, 9, 21
Popinchalk, M., Faherty, J. K., Kiman, R., et al. 2021, ApJ, 916, 77
Rafikov, R. R., & Silsbee, K. 2015a, ApJ, 798, 69
Rafikov, R. R., & Silsbee, K. 2015b, ApJ, 798, 70
Raghavan, D., McAlister, H. A., Henry, T. J., et al. 2010, ApJS, 190, 1
Ricker, G. R., Winn, J. N., Vanderspek, R., et al. 2015, JATIS, 1, 014003
Riedel, A. R., Subasavage, J. P., Finch, C. T., et al. 2010, AJ, 140, 897
Salama, M., Ou, J., Baranec, C., et al. 2021, AJ, 162, 102
Scott, N. J., Howell, S. B., Horch, E. P., & Everett, M. E. 2018, PASP, 130, 054502
Shields, Aomawa L., Ballard, Sarah, & Johnson, John Asher 2016, PhR, 663, 1
Skrutskie, M. F., Cutri, R. M., Stiening, R., et al. 2006, AJ, 131, 1163
Skrutskie, M. F., Cutri, R. M., Stiening, R., et al. 2019, 2MASS All-Sky Point Source Catalog, IPAC, doi:10.26131/IRSA2
Tokovinin, A. 2023, AJ, 165, 180
Torres, G., Andersen, J., & Giménez, A. 2010, A&ARv, 18, 67
van Altena, W. F., Lee, J. T., & Hoffleit, E. D. 1995, The General Catalogue of Trigonometric [Stellar] Parallaxes (New Haven, CT: Yale Univ. Obs.)
van Leeuwen, F. 2007, A&A, 474, 653
Virtanen, P., Gommers, R., Oliphant, T. E., et al. 2020, NatMe, 17, 261
Vrijmoet, E. H., Henry, T. J., Jao, W.-C., & Dieterich, S. B. 2020, AJ, 160, 215
Vrijmoet, E. H., Tokovinin, A., Henry, T. J., et al. 2022, AJ, 163, 178
Ward-Duong, K., Patience, J., De Rosa, R. J., et al. 2015, MNRAS, 449, 2618
Waters, C., Magnier, E. A. & Pan-STARRS Science Consortium 2015, IAUGA, 29, 2256019
Weinberger, A. J., Boss, A. P., Keiser, S. A., et al. 2016, AJ, 152, 24
Winters, J. G., Charbonneau, D., Henry, T. J., et al. 2021, AJ, 161, 63
Winters, J. G., Henry, T. J., Jao, W.-C., et al. 2019, AJ, 157, 216
Winters, J. G., Henry, T. J., Lurie, J. C., et al. 2015, AJ, 149, 5
Winters, J. G., Sevrinsky, R. A., Jao, W.-C., et al. 2017, AJ, 153, 14
Ziegler, C., Tokovinin, A., Briceño, C., et al. 2020, AJ, 159, 19

The Astronomical Journal, 168:229 (2pp), 2024 November https://doi.org/10.3847/1538-3881/ad7eb3

Erratum: "The POKEMON Speckle Survey of Nearby M Dwarfs. II. Observations of 1125 Targets" (2024, AJ, 167, 56)

Catherine A. Clark[1], Gerard T. van Belle[2], Elliott P. Horch[3], Michael B. Lund[1], David R. Ciardi[1], Kaspar von Braun[2], Jennifer G. Winters[4,5], Mark E. Everett[6], Zachary D. Hartman[7], and Joe Llama[2]
[1] NASA Exoplanet Science Institute, IPAC, California Institute of Technology, Pasadena, CA 91125, USA; clarkc@ipac.caltech.edu
[2] Lowell Observatory, 1400 West Mars Hill Road, Flagstaff, AZ 86001, USA
[3] Southern Connecticut State University, 501 Crescent Street, New Haven, CT 06515, USA
[4] Bridgewater State University, 131 Summer Street, Bridgewater, MA 02324, USA
[5] Center for Astrophysics, Harvard & Smithsonian, 60 Garden Street, Cambridge, MA 02138, USA
[6] NSF's National Optical-Infrared Astronomy Research Laboratory, 950 N. Cherry Avenue, Tucson, AZ 85719, USA
[7] Gemini Observatory/NSF's NOIRLab, 670 A'ohoku Place, Hilo, HI 96720, USA
Received 2024 September 20; published 2024 October 31

Materials only available in the online version of record: machine-readable tables

We have discovered that one of the stellar companions that was cataloged in C. A. Clark et al. (2024a) was in fact a spurious detection during one of the 5000 40 ms exposures.

We detected a stellar companion to GJ 369 at 0.″4497 and a position angle of 38.°5 on UT 2017 May 7 using the Differential Speckle Survey Instrument (E. P. Horch et al. 2009) at the 4.3 m Lowell Discovery Telescope outside Flagstaff, Arizona. The companion was detected at 880 nm with a delta magnitude of <3.30.

However, observations of GJ 369 from UT 2016 January 14 show that the star is in fact single (J. G. Winters et al. 2024, in preparation). In the 2017 observations, there was a double cosmic-ray hit in Frame 4645 of 5000, inducing an artifact in the final reconstructed image that masqueraded as a binary in the summed power spectrum.

The 2017 observations have now been reanalyzed and show that GJ 369 is single, in agreement with the observations from 2016. We include updates to Tables 1 and 4 here.

Because GJ 369 is within 15 pc ($\pi = 76.2$ mas; Gaia Collaboration et al. 2023), it was also included in C. A. Clark et al. (2024b) and will be discussed in an erratum for that publication as well.

Table 1
POKEMON Targets

2MASS ID or Name	Gaia DR3 ID	G Magnitude (mag)	G_{RP} Magnitude (mag)	Distance (pc)	References	RUWE	IPDFMP	Companion(s) Detected?
00051079+4547116	386655019234959872	9.1	8.0	11.5	(8)	1.0	0	N
00054090+4548374	386653747925624576	8.3	7.4	11.5	(8)	1.2	2	N
00064325-0732147	2441630500517079808	11.8	10.4	4.8	(8)	1.3	4	N
00074264+6022543	429297924157113856	12.4	10.7	15.4	(8)	3.9	72	Y
00085391+2050252	2798766647610195456	12.0	10.7	18.1	(7)	…	8	Y
00085512+4918561	393621524910343296	14.4	13.0	14.8	(8)	1.1	0	N
00113182+5908400	423027104407576576	13.5	12.1	9.3	(8)	1.1	0	N
00152799-1608008	2368293487261055488	10.3	8.9	5.0	(16)	…	60	Y
00153905+4735220	392350008432819328	10.0	8.9	11.5	(8)	0.9	3	N
00154919+1333218	2768048564768256512	11.4	10.2	12.2	(8)	1.2	0	N

References: (1) C. Cifuentes et al. (2020); (2) J. A. Dittmann et al. (2014); (3) T. J. Dupuy & M. C. Liu (2017); (4) T. J. Dupuy et al. (2019); (5) C. T. Finch & N. Zacharias (2016); (6) C. T. Finch et al. (2018); (7) Gaia Collaboration et al. (2018); (8) Gaia Collaboration et al. (2023); (9) W. Gliese & H. Jahreiß (1991); (10) T. Henry et al. (2006); (11) S. Lépine et al. (2009); (12) C. A. Murray et al. (1986); (13) A. R. Riedel et al. (2010); (14) G. Torres et al. (2010); (15) W. F. van Altena et al. (1995); (16) F. van Leeuwen (2007); (17) A. J. Weinberger et al. (2016); (18) J. G. Winters et al. (2015); (19) J. G. Winters et al. (2017).

(This table is available in its entirety in machine-readable form in the online article.)

Table 4
Properties of Companions Detected throughout the POKEMON Survey

2MASS ID or Name	WDS ID	Epoch (2000+)	λ (nm)	$\Delta\lambda$ (nm)	θ_1 (deg)	ρ_1 (arcsec)	Δm_1 (mag)	θ_2 (deg)	ρ_2 (arcsec)	Δm_2 (mag)
00074264+6022543	00077+6022	18.5887	562	44	107.6	0.9750	0.95	…	…	…
		18.5887	832	40	107.9	0.9774	0.76	…	…	…
00085391+2050252	00089+2050	18.5853	832	40	232.4	0.1329	0.64	…	…	…
00152799-1608008	00155-1608	17.8025	692	40	131.6	0.1944	2.46	…	…	…
		17.8025	880	50	131.1	0.1910	1.64	…	…	…
		18.6571	832	40	4.8	0.2146	1.58	…	…	…
00244419-2708242	00247-2653	18.6571	832	40	51.7	0.9122	<2.41	…	…	…
00322970+6714080	00321+6715	18.5887	562	44	354.7	0.4695	3.94	185.4	3.5795	<2.78
		18.5887	832	40	355.3	0.4806	3.05	185.6	3.5909	<2.46
		19.0643	832	40	3.8	0.4941	2.44	…	…	…

Note. Astrometric and photometric uncertainties are described in Sections 3.2 and 3.3 of the original paper (Clark et al. 2024a), respectively.

(This table is available in its entirety in machine-readable form in the online article.)

ORCID iDs

Catherine A. Clark https://orcid.org/0000-0002-2361-5812
Gerard T. van Belle https://orcid.org/0000-0002-8552-158X
Elliott P. Horch https://orcid.org/0000-0003-2159-1463
Michael B. Lund https://orcid.org/0000-0003-2527-1598
David R. Ciardi https://orcid.org/0000-0002-5741-3047
Kaspar von Braun https://orcid.org/0000-0002-5823-4630
Jennifer G. Winters https://orcid.org/0000-0001-6031-9513
Mark E. Everett https://orcid.org/0000-0002-0885-7215
Zachary D. Hartman https://orcid.org/0000-0003-4236-6927
Joe Llama https://orcid.org/0000-0003-4450-0368

References

Cifuentes, C., Caballero, J. A., Cortés-Contreras, M., et al. 2020, A&A, 642, A115
Clark, C. A., van Belle, G. T., Horch, E. P., et al. 2024a, AJ, 167, 56
Clark, C. A., van Belle, G. T., Horch, E. P., et al. 2024b, AJ, 167, 174
Dittmann, J. A., Irwin, J. M., Charbonneau, D., & Berta-Thompson, Z. K. 2014, ApJ, 784, 156
Dupuy, T. J., & Liu, M. C. 2017, ApJS, 231, 15
Dupuy, T. J., Liu, M. C., Best, W. M. J., et al. 2019, AJ, 158, 174
Finch, C. T., & Zacharias, N. 2016, AJ, 151, 160
Finch, C. T., Zacharias, N., & Jao, W.-C. 2018, AJ, 155, 176
Gaia Collaboration, Brown, A. G. A., Vallenari, A., et al. 2018, A&A, 616, A1
Gaia Collaboration, Vallenari, A., Brown, A. G. A., et al. 2023, A&A, 674, A1
Gliese, W., & Jahreiß, H. 1991, in Preliminary Version of the Third Catalogue of Nearby Stars, On: The Astronomical Data Center CD-ROM: Selected Astronomical Catalogs, ed. L. E. Brotzmann & S. E. Gesser, Vol. I (Greenbelt, MD: NASA/Astronomical Data Center, Goddard Space Flight Center)
Henry, T., Jao, W.-C., Subasavage, J., et al. 2006, AJ, 132, 2360
Horch, E. P., Veillette, D. R., Baena Galle, R., et al. 2009, AJ, 137, 5057
Lépine, S., Thorstensen, J. R., Shara, M. M., & Rich, R. M. 2009, AJ, 137, 4109
Murray, C. A., Argyle, R. W., & Corben, P. M. 1986, MNRAS, 223, 629
Riedel, A. R., Subasavage, J. P., Finch, C. T., et al. 2010, AJ, 140, 897
Torres, G., Andersen, J., & Giménez, A. 2010, A&ARv, 18, 67
van Altena, W. F., Lee, J. T., & Hoffleit, E. D. 1995, The General Catalogue of Trigonometric [Stellar] Parallaxes (New Haven, CT: Yale Univ. Obs.)
van Leeuwen, F. 2007, A&A, 474, 653
Weinberger, A. J., Boss, A. P., Keiser, S. A., et al. 2016, AJ, 152, 24
Winters, J. G., Henry, T. J., Lurie, J. C., et al. 2015, AJ, 149, 5
Winters, J. G., Sevrinsky, R. A., Jao, W.-C., et al. 2017, AJ, 153, 14